arXiv:1412.1390v1 [q-bio.CB] 25 Nov 2014

Growth-dependent bacterial susceptibility to ribosome-targeting antibiotics

Philip Greulich[1,2], Matthew Scott[3], Martin R. Evans[2]
and Rosalind J. Allen[2]

1: Cavendish Laboratory, University of Cambridge, J J Thompson Avenue, Cambridge CB3 0HE, United Kingdom

2: SUPA, School of Physics and Astronomy, University of Edinburgh, James Clerk Maxwell Building, Peter Guthrie Tait Road, Edinburgh EH9 3FD, United Kingdom

3: Department of Applied Mathematics, University of Waterloo, Waterloo, Ontario N2L 3G1 Canada

Corresponding author: Rosalind J. Allen, rallen2@staffmail.ed.ac.uk

Abstract

Bacterial growth environment strongly influences the efficacy of antibiotic treatment, with slow growth often being associated with decreased susceptibility. Yet in many cases the connection between antibiotic susceptibility and pathogen physiology remains unclear. We show that for ribosome-targeting antibiotics acting on *Escherichia coli*, a complex interplay exists between physiology and antibiotic action; for some antibiotics within this class faster growth indeed increases susceptibility, but for other antibiotics the opposite is true. Remarkably, these observations can be explained by a simple mathematical model that combines drug transport and binding with physiological constraints. Our model reveals that growth-dependent susceptibility is controlled by a single parameter characterizing the 'reversibility' of antibiotic transport and binding. This parameter provides a spectrum-classification of antibiotic growth-dependent efficacy that appears to correspond at its extremes to existing binary classification schemes. In these limits the model predicts universal, parameter-free limiting forms for growth inhibition curves. The model also leads to non-trivial predictions for the drug susceptibility of a translation-mutant strain of *E. coli*, which we verify experimentally. Drug action and bacterial metabolism are mechanistically complex; nevertheless this study illustrates how coarse-grained models can be used to integrate pathogen physiology into drug design and treatment strategies.

Introduction

Quantitative predictions for the inhibition of bacterial growth by antibiotics are essential for the design of treatment strategies [1] and for controlling the evolution of antibiotic resistance [2–5]. The efficacy of antibiotic treatment can be strongly affected by changes in pathogen physiology, such as biofilm formation [6], switching to persister states [7], and responses to metabolic stimuli [8]; with slow bacterial growth often being associated with decreased antibiotic susceptibility [9–11]. Yet, despite its importance, in most cases the connection between bacterial physiology and antibiotic susceptibility remains unclear. Here we show that for ribosome-targeting antibiotics in *Escherichia coli* a strong correlation exists between physiology, controlled by the nutrient quality of the growth environment, and antibiotic susceptibility.

Ribosome-targeting antibiotics constitute a major class of antibacterial drugs in current clinical use. Within this class, different drugs bind to different ribosomal target sites, inhibit different aspects of ribosome function and may bind to their target with varying degrees of reversibility [12, 13]. We investigate four different ribosome-targeting antibiotics, two of which bind almost irreversibly, and two of which bind reversibly. Specifically, streptomycin and kanamycin are aminoglycosides which bind irreversibly to the 30S ribosomal complex, inhibiting initiation and inducing mistranslation [14]. We also study the reversibly-binding drugs tetracycline, which targets the 30S complex, inhibiting the binding of aminoacyl tRNA [15], and chloramphenicol, which targets the 50S ribosomal complex, preventing peptide bond formation [16, 17]. We find that the efficacies of these antibiotics exhibit qualitatively different responses to changes in the bacterial growth environment.

It has long been known that the ribosome content of a bacterial cell correlates closely with its growth rate under conditions of exponential growth [18, 19]. Recently, it has been shown that this phenomenon can be understood as a growth-rate dependent partitioning of the cell's translational resources between production of new ribosomes and production of other proteins [20, 21]. This partitioning can be described by a set of empirically-determined constraints, analogous to the rules that govern the behaviour of electric circuits [20, 22]. Empirical growth constraints provide a physiological chassis into which mechanistic models for the expression of synthetic gene circuits, or endogenous genes, have been integrated [23, 24].

The fact that the cell's ribosome content is growth-rate dependent suggests that the efficacy of ribosome-targeting antibiotics should likewise exhibit growth-rate dependence. We demonstrate that bacterial susceptibility to ribosome-targeting antibiotics does indeed depend strongly on the nutrient environment as characterized by the bacterial growth rate prior to antibiotic treatment. Surprisingly, although the four antibiotics used in our study share the same target, we observe contrasting forms for the efficacy-growth rate relations of different antibiotics.

These intriguing results can be explained by a simple mathematical model for antibiotic transport and ribosome binding which incorporates the empirical growth constraints; growth inhibition relations which are predicted by the model are in quantitative agreement with our data for both wild type and mutant strains of *E. coli*. A single dimensionless parameter, which characterizes the reversibility of transport and binding relative to the drug-free growth rate, emerges from our analysis, providing a simple way to predict how changes in antibiotic chemistry, pathogen genetics or physiological state will affect drug response. This 'reversibility parameter' provides a robust classification of ribosome-targeting antibiotics according to their growth-rate efficacy relations, with implications for clinical practice and for the evolution of antibiotic resistance. In particular, reversible antibiotics are predicted to work better on fast-growing infections, whereas irreversible antibiotics are more effective for slow-growing pathogens. From a wider perspective, the approach taken here, in which empirical physiological constraints are coupled with models for molecular mode-of-action, could reveal similar surprising growth-rate efficacy relations in other classes of antibiotics.

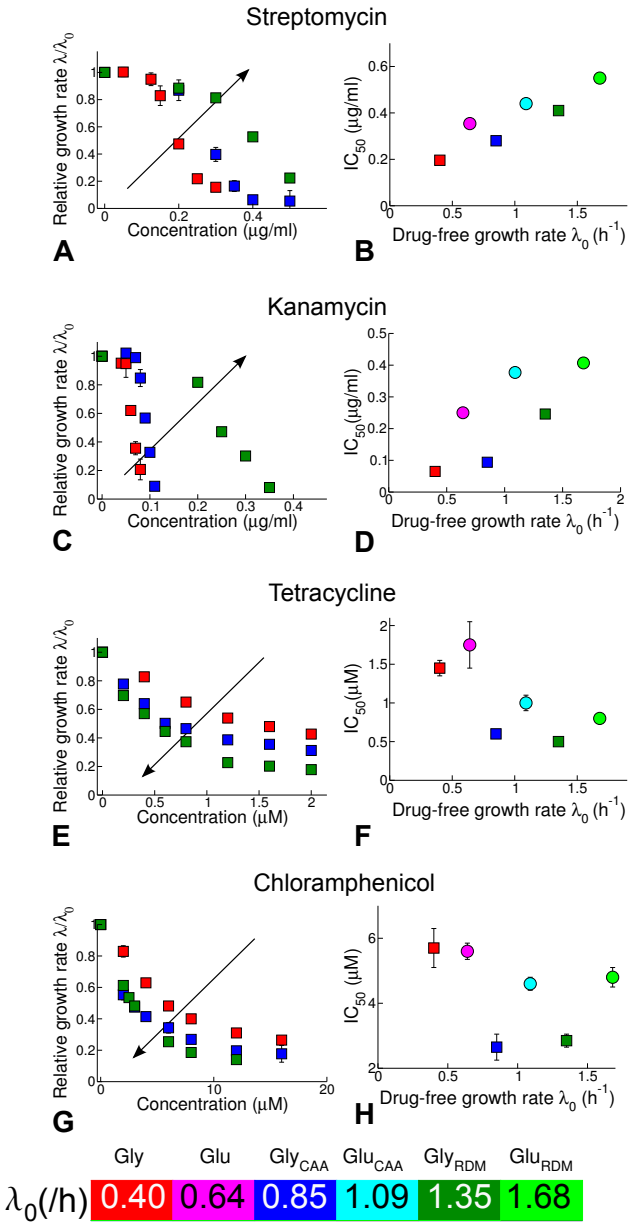

FIG. 1: Antibiotic susceptibility depends on nutrient quality for four ribosome-targeting antibiotics: irreversibly-binding antibiotics streptomycin (**A** & **B**) and kanamycin (**C** & **D**), and reversibly-binding antibiotics tetracycline (**E** & **F**) and chloramphenicol (**G** & **H**). The left panels show the growth rate λ of *E. coli* MG1655 relative to the drug-free growth rate λ_0, as a function of the antibiotic concentration. Growth inhibition data are shown for media with glycerol as the carbon source. The arrows indicate increasing drug-free growth rate λ_0. The right panels show the half-inhibition concentration IC_{50} as a function of the drug-free growth rate λ_0. Carbon sources are denoted by symbol: glucose (circles), glycerol (squares), and error bars denote the standard deviation among repeated measurements (Tables S2 and S3). Media are variants of Neidhardt's MOPS buffered medium [25]; see Methods for details.

Results

Antibiotic efficacy depends on growth rate

To investigate the link between bacterial growth environment and susceptibility to ribosome-targeting antibiotics, we measured growth inhibition curves (exponential growth rate as a function of antibiotic concentration) for *E. coli* cells on media of increasing nutrient quality. As the nutrient quality increases, so too does the 'drug-free growth rate' λ_0, *i.e.* the exponential growth rate in the absence of antibiotic (Fig. 1, colorbar and Table S1). For the four ribosome-targeting antibiotics streptomycin, kanamycin, tetracycline and chloramphenicol, the growth inhibition curves indeed exhibit a strong dependence on the drug-free growth rate λ_0 (Fig. 1, left panels and Table S2).

Bacterial susceptibility to antibiotic can be quantified by the IC_{50}: the antibiotic concentration needed to halve the bacterial growth rate. Plotting the IC_{50} as a function of the drug-free growth rate λ_0, we observe contrasting trends between antibiotics (Fig. 1, right panels and Table S3). For the irreversibly-binding antibiotics streptomycin and kanamycin, the IC_{50} increases with nutrient quality, *i.e.* faster-growing cells are less susceptible to antibiotic. In contrast, for the reversibly-binding antibiotics tetracycline and chloramphenicol, the IC_{50} predominantly decreases as nutrient quality increases, *i.e.* faster-growing cells are more susceptible to antibiotic treatment. Data sets for glycerol and glucose-based media show distinct trends in IC_{50} with drug-free growth rate. The shapes of the growth inhibition curves also differ markedly between the two groups of antibiotics: we observe threshold-like inhibition, *i.e.* a sharp decrease in growth rate, for streptomycin and kanamycin (Fig. 1A & C), and more gradual inhibition for tetracycline and chloramphenicol (Fig. 1E & G). Despite having similar targets, these antibiotics appear to respond to changes in cell physiology in very different ways.

Mathematical model

Our experimental data can be explained by a simple mathematical model. In our model, antibiotic molecules enter a bacterial cell and bind to ribosomes, while at the same time, new ribosomes are synthesized and the cell contents are diluted by growth. Our model is placed within a physiological context via the empirical growth constraints [20, 22].

In the model, the state of the cell is described by the intracellular concentration of an-

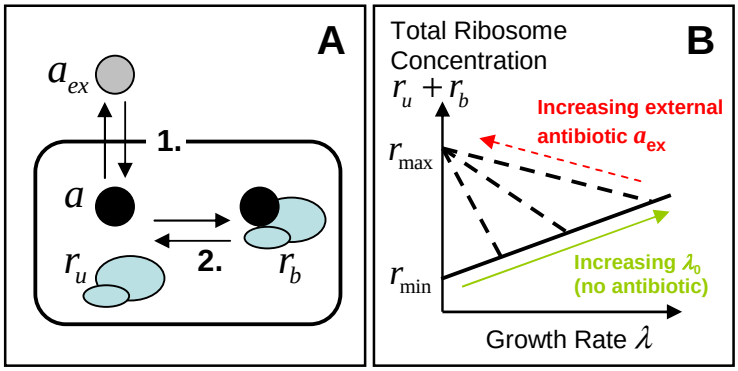

FIG. 2: Schematic view of the model and its dynamics. **A.** The model is focused on three state variables: the intracellular concentration of antibiotic a, the concentration r_{u} of ribosomes unbound by antibiotic and the concentration r_{b} of antibiotic-bound ribosomes. Two mechanisms drive the dynamics: 1. *Transport* across the cell membrane and 2. *Binding* of ribosomes and antibiotic. **B.** Constraints arising from empirical relations between ribosome content and growth rate. Scott *et al.* [20] measured total ribosome content as a function of growth rate. When growth rate is varied by nutrient composition, in the absence of antibiotics, ribosome content r_{u} correlates positively with growth rate λ, increasing linearly from a minimum concentration of inactive ribosomes r_{min} (solid line). When growth rate is decreased by imposing translational inhibition, total ribosome content $r_{\mathrm{tot}} = r_{\mathrm{u}} + r_{\mathrm{b}}$ increases, reaching a maximum r_{max} as growth rate decreases to zero (dashed lines). Note that Scott *et al.* measured ribosome mass fraction; here we translate these to concentrations (see Supplementary Information, Fig. S1).

tibiotic a, the concentration r_{u} of ribosomes unbound by antibiotic and the concentration r_{b} of antibiotic-bound ribosomes (Fig. 2A). Two mechanisms drive the dynamics: 1. transport of extracellular antibiotic a_{ex} into the cell at rate $J(a_{\mathrm{ex}}, a) = P_{\mathrm{in}} a_{\mathrm{ex}} - P_{\mathrm{out}} a$, where P_{in} and P_{out} quantify the permeability of the cell membrane in the inward and outward directions; and 2. binding of ribosomes and antibiotic $f(r_{\mathrm{u}}, r_{\mathrm{b}}, a) = -k_{\mathrm{on}}\, a\, (r_{\mathrm{u}} - r_{\mathrm{min}}) + k_{\mathrm{off}}\, r_{\mathrm{b}}$, with binding and unbinding rate constants k_{on} and k_{off}, respectively, and equilibrium dissociation constant $K_{\mathrm{D}} = k_{\mathrm{off}}/k_{\mathrm{on}}$ (the inactive fraction r_{min} is assumed not to bind the antibiotic). In exponential growth, cell contents are diluted at rate λ, new ribosomes are synthesized at

rate $s(\lambda)$, and the dynamics of the system are governed by the following equations:

$$\frac{da}{dt} = -\lambda\, a + f(r_{\rm u}, r_{\rm b}, a) + J(a_{\rm ex}, a), \tag{1}$$

$$\frac{dr_{\rm u}}{dt} = -\lambda\, r_{\rm u} + f(r_{\rm u}, r_{\rm b}, a) + s(\lambda), \tag{2}$$

$$\frac{dr_{\rm b}}{dt} = -\lambda\, r_{\rm b} - f(r_{\rm u}, r_{\rm b}, a). \tag{3}$$

This model is coupled to cell physiology via the empirical relations of Scott *et al* [20], which link the growth rate λ and ribosome synthesis rate $s(\lambda)$ to the ribosome concentration; these act as constraints on the dynamical equations 1-3. The first empirical growth constraint states that the unbound ribosome content $r_{\rm u}$ and the growth rate λ are linearly proportional:

$$r_{\rm u} = \lambda/\kappa_{\rm t} + r_{\rm min}. \tag{4}$$

Here, $r_{\rm min} = 19.3\mu$M is the minimal unbound ribosome content needed for growth and the translational capacity $\kappa_{\rm t} = 0.06\mu{\rm M}^{-1}{\rm h}^{-1}$ is related to the maximum peptide elongation rate [26]. This relation emerges from experiments in which the growth rate is varied by changing the nutrient source in the absence of antibiotic (green arrow in Fig. 2B; see also the Supplementary Information). The second empirical growth constraint describes how the ribosome content is upregulated in response to translational inhibition. Upon decreasing the growth rate by translational inhibition (for a fixed nutrient source), the total ribosome content $r_{\rm tot}$ increases linearly, reaching a fixed maximal value $r_{\rm max} = 65.8\mu$M as $\lambda \to 0$ [20] (red arrow in Fig. 2B; see also the Supplementary Information). This can be expressed mathematically as

$$r_{\rm tot} = r_{\rm u} + r_{\rm b} = r_{\rm max} - \lambda\Delta r \left(\frac{1}{\lambda_0} - \frac{1}{\kappa_{\rm t}\Delta r}\right), \tag{5}$$

where $\Delta r = r_{\rm max} - r_{\rm min} = 46.5\mu$M is the dynamic range of the ribosome concentration. The implication of the second empirical growth constraint, Eq. 5, is that cells that are initially growing more slowly have a greater capacity to upregulate their ribosome content upon antibiotic challenge (steeper slope of the dashed line in Fig. 2B) than those that are initially growing fast; *i.e.*, slowly growing cells can increase their ribosome content with little resulting change in their growth rate. Adding together Eqs 2 and 3 at steady state ($dr_{\rm u}/dt = dr_{\rm b}/dt = 0$) shows that the ribosome synthesis rate $s(\lambda)$ is the product of growth rate and total ribosome content,

$$s(\lambda) = \lambda r_{\rm tot} = \lambda\left[r_{\rm max} - \lambda\Delta r\left(\frac{1}{\lambda_0} - \frac{1}{\kappa_{\rm t}\Delta r}\right)\right]. \tag{6}$$

Quantitative results for growth-inhibition curves

Solving the model equations 1-3 at steady state, together with the physiological constraints, Eqs 4 and 5, produces a universal equation that links the steady-state relative growth rate λ/λ_0 to the extracellular antibiotic concentration $a_{\rm ex}$ (see Supplementary Information; here we have assumed that the antibiotic binding rate $k_{\rm on}$ typically exceeds the translational capacity $\kappa_{\mathbf{t}}$ by several orders of magnitude, $k_{\rm on} \gg \kappa_{\mathbf{t}}$). This equation is

$$0 = \left(\frac{\lambda}{\lambda_0}\right)^3 - \left(\frac{\lambda}{\lambda_0}\right)^2 + \left(\frac{\lambda}{\lambda_0}\right)\left[\frac{1}{4}\left(\frac{\lambda_0^*}{\lambda_0}\right)^2 + \frac{a_{\rm ex}}{2\,{\rm IC}_{50}^*}\left(\frac{\lambda_0^*}{\lambda_0}\right)\right] - \frac{1}{4}\left(\frac{\lambda_0^*}{\lambda_0}\right)^2. \tag{7}$$

Remarkably, Eq. 7 states that the growth-dependent antibiotic susceptibility is controlled by only two parameter combinations, defined as follows: a rate λ_0^*, which characterizes the reversibility of antibiotic transport and binding:

$$\lambda_0^* = 2\sqrt{P_{\rm out}\kappa_t K_D}, \tag{8}$$

and a concentration scale

$${\rm IC}_{50}^* = \frac{\Delta r \lambda_0^*}{2P_{\rm in}}. \tag{9}$$

In the model, λ_0^* is used to normalize the drug-free growth rate λ_0 and ${\rm IC}_{50}^*$ is used to normalize the extracellular antibiotic concentration $a_{\rm ex}$, and later the half-inhibition concentration ${\rm IC}_{50}$.

Predictions for growth inhibition curves can be obtained by solving Eq. 7; the shapes of these curves depend only on the value of λ_0^*. For small values of λ_0^* (the irreversible limit), the model predicts a discontinuous drop in growth rate at the ${\rm IC}_{50}$, as we see in our data for streptomycin and kanamycin (Fig. 1 and Fig. 3). Interestingly, in this case the model predicts a bistable dependence of growth rate on antibiotic concentration at the level of individual cells (Fig. S2). For larger values of λ_0^* (the reversible limit), the model instead predicts a smooth decrease in growth rate over a wide range of antibiotic concentrations, as we observe for tetracycline and chloramphenicol (Fig. S2, Fig. 1 and Fig. 3).

Fitting the model to the data via the parameters λ_0^* and ${\rm IC}_{50}^*$ yields excellent agreement for tetracycline and chloramphenicol, and reasonable agreement for streptomycin and kanamycin (Fig. 3). In all cases, the fitted parameters λ_0^* and ${\rm IC}_{50}^*$ differ between the

two carbon sources (Table S3), suggesting carbon-source effects on transporter-mediated influx and outflux ($P_{\rm in}$ and $P_{\rm out}$, respectively) [8]. The fitted parameters are in good agreement with biochemical parameter values available from literature data (Table S4) and are consistent with the fact that aminoglycosides are believed to bind and be transported irreversibly (small λ_0^*) [14], whereas for tetracycline and chloramphenicol both transport and binding processes are reversible (λ_0^*) [17, 27]. For kanamycin the agreement is less accurate than for streptomycin; this deviation may be ascribed to the presence of an additional binding site on the ribosome with comparable affinity [28, 29], a property not considered in our model. Nonetheless, our model correctly predicts the sigmoidal form of kanamycin's growth-inhibition curve and the decreasing susceptibility with growth rate.

Universal growth-dependent antibiotic susceptibility curve

One of the major insights provided by the model is a simple explanation for the contrasting trends in growth-dependent susceptibility for different antibiotics which we observe in our experiments. Substituting $a_{\rm ex} = {\rm IC}_{50}$ and $\lambda = \lambda_0/2$ into Eq. 7, we find that, for all antibiotics, the growth-rate dependence of the half-inhibition concentration ${\rm IC}_{50}$ is predicted to fall onto a universal 'growth-dependent susceptibility' curve

$$\frac{{\rm IC}_{50}}{{\rm IC}_{50}^*} = \frac{1}{2}\left[\frac{\lambda_0}{\lambda_0^*} + \frac{\lambda_0^*}{\lambda_0}\right]. \tag{10}$$

Eq. 10 is derived in the Supplementary Information and holds for $k_{\rm on} \gg \kappa_t$. Rescaling our data using the values of λ_0^* and ${\rm IC}_{50}^*$ obtained from the growth-inhibition curve fits of Fig. 3 (and the equivalent fit for the glucose-based media; Table S3), Figure 4 shows that our data indeed collapse on to this universal curve.

If the drug-free growth rate λ_0 exceeds the critical reversibility rate λ_0^*, the model (Eq. 10) predicts that the ${\rm IC}_{50}$ will increase with λ_0; *i.e.* fast-growing cells will be less susceptible, as we observe for streptomycin and kanamycin. In contrast, if the drug-free growth rate λ_0 is less than the critical reversibility rate λ_0^*, Eq. 10 predicts that the ${\rm IC}_{50}$ will decrease as λ_0 increases; *i.e.* fast-growing cells will be more susceptible, as we observe for tetracycline and chloramphenicol. The critical parameter ${\rm IC}_{50}^*$ provides a growth-rate independent scale for the extracellular antibiotic concentration; we find that an antibiotic concentration $a_{\rm ex} > {\rm IC}_{50}^*$ is required for effective growth inhibition, regardless of the drug-free growth rate.

The universal growth-dependent susceptibility curve, Eq. 10 (Fig. 4), suggests that the

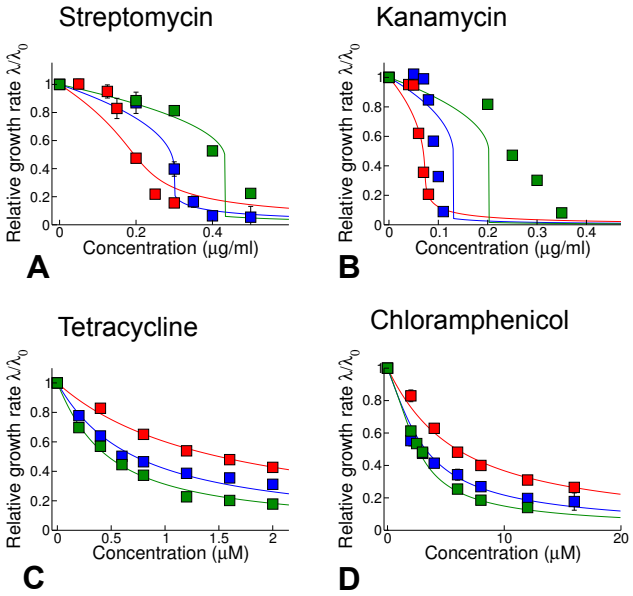

FIG. 3: Model fits to growth inhibition curve data. The parameters λ_0^* and IC_{50}^* are obtained by numerical fitting of the solution of the cubic equation, Eq. 7, to our experimental growth inhibition curves. Data sets for different drug-free growth rates (*i.e.* the different curves in each panel) were fitted simultaneously with the same values of λ_0^* and IC_{50}^*, but separate fits were obtained for glycerol-based and glucose-based media. Here we show the resulting fits for glycerol-based media (symbols as in Fig. 1.). The parameters obtained by this procedure are: Streptomycin, glycerol: $\lambda_0^* = 0.31\mathrm{h}^{-1}$, $\mathrm{IC}_{50}^* = 0.19\mu\mathrm{g/ml}$, streptomycin, glucose: $\lambda_0^* = 0.57\mathrm{h}^{-1}$, $\mathrm{IC}_{50}^* = 0.36\mu\mathrm{g/ml}$, kanamycin, glycerol: $\lambda_0^* = 0.17\mathrm{h}^{-1}$, $\mathrm{IC}_{50}^* = 0.05\mu\mathrm{g/ml}$, kanamycin, glucose: $\lambda_0^* = 0.47\mathrm{h}^{-1}$, $\mathrm{IC}_{50}^* = 0.26\mu\mathrm{g/ml}$, tetracycline, glycerol: $\lambda_0^* = 5.2\mathrm{h}^{-1}$, $\mathrm{IC}_{50}^* = 0.23\mu\mathrm{M}$, tetracycline, glucose: $\lambda_0^* = 6.3\mathrm{h}^{-1}$, $\mathrm{IC}_{50}^* = 0.36\mu\mathrm{M}$, chloramphenicol, glycerol: $\lambda_0^* = 1.8\mathrm{h}^{-1}$, $\mathrm{IC}_{50}^* = 2.5\mu\mathrm{M}$, chloramphenicol, glucose: $\lambda_0^* = 1.5\mathrm{h}^{-1}$, $\mathrm{IC}_{50}^* = 4.1\mu\mathrm{M}$. These values of λ_0^* and IC_{50}^* are compared to literature data in Table S4. Similar results are obtained if we instead fit our data directly to the predicted universal relation for $\mathrm{IC}_{50}(\lambda_0)$ (Eq. 10); see Supplementary Information and Fig. S3.

ratio (λ_0/λ_0^*) of the drug-free growth rate λ_0 to the 'reversibility' rate $\lambda_0^* = \sqrt{\kappa_t P_{\mathrm{out}} k_{\mathrm{off}}}$ provides a natural spectrum classification of antibiotic action, integrating growth environment (through λ_0) with antibiotic chemistry and pathogen genetics (through the molecular parameters which are combined in λ_0^*). Drug-pathogen interactions characterized by small values of λ_0^* are predicted to behave like our irreversible antibiotics (streptomycin and

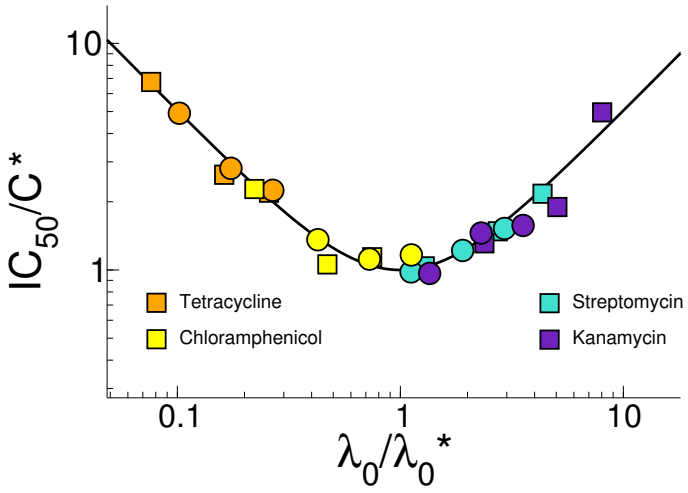

FIG. 4: Universal growth-dependent susceptibility curve. Data from the right panels of Fig. 1 are rescaled by λ_0^* and IC_{50}^*, obtained by fitting our growth inhibition data (Fig. 3). The black line shows the model prediction for the universal curve, Eq. 10.

kanamycin); showing decreased efficacy under rich nutrient conditions. Drug-pathogen interactions characterized by large values of λ_0^* are expected to behave like the reversible antibiotics in our study (chloramphenicol and tetracycline); showing increased efficacy under rich nutrient conditions. Drugs with values of λ_0^* close to the drug-free growth rate λ_0 achievable in experiments may show non-monotonically varying susceptibility as nutrient quality is varied; our data suggest this may in fact be the case for chloramphenicol (Fig. 1H), in agreement with literature-value estimates for λ_0^* (Table S4). Low outward permeability has been implicated in growth bistability and masking of resistance mutations [30, 31] (see in particular the discussion of Ref.[30] in the Supplementary Text); we propose that irreversibility in binding and transport is a major determinant of growth-dependent antibiotic susceptibility.

Simple predictions in the reversible and irreversible limits

In the limiting cases of very large or very small λ_0^*, *i.e.* the limits in which antibiotic transport and binding is either fully reversible or fully irreversible, the model leads to simple predictions for the growth inhibition curve and growth-rate dependence of the half-inhibition concentration IC_{50}. For small λ_0^* (the irreversible limit), a qualitatively different, discontin-

uous, form for the growth inhibition curve is predicted by Eq. 7:

$$\frac{\lambda}{\lambda_0} = \frac{1}{2}\left[1 + \sqrt{1 - \frac{a_{\rm ex}}{\rm IC_{50}}}\ \right], \tag{11}$$

for $a_{\rm ex} < {\rm IC}_{50}$ and zero for $a_{\rm ex} > {\rm IC}_{50}$. In this case, the ${\rm IC}_{50} = {\rm IC}^*_{50}\lambda_0/(2\lambda^*_0) = \lambda_0\Delta r/(4P_{\rm in})$ increases linearly with the drug-free growth rate λ_0 (see Supplementary Information). For large λ^*_0 (the reversible limit), the growth inhibition curve obtained from solving Eq. 7 is given by the smoothly-varying, Langmuir form:

$$\frac{\lambda}{\lambda_0} = \frac{1}{1 + a_{\rm ex}/{\rm IC}_{50}}, \tag{12}$$

where $a_{\rm ex}$ is the extracellular antibiotic concentration and the ${\rm IC}_{50} = {\rm IC}^*_{50}\lambda^*_0/(2\lambda_0) = K_D \times (P_{\rm out}/P_{\rm in}) \times (\kappa_t\Delta r/\lambda_0)$ is inversely proportional to the drug-free growth rate λ_0 (see Supplementary Information).

Scaling all our growth inhibition curves by the drug-free growth rate λ_0 and the half-inhibition concentration ${\rm IC}_{50}$ we find that our combined data sets for the reversible and irreversible drugs collapse onto these two qualitatively distinct, parameter-free curves, as predicted by the model (Fig. 5) – although, as expected, the quantitative agreement with the limiting-case theoretical prediction is not quite as good as with the full solution of the cubic equation (Fig. 3).

Testing the model predictions for a translation mutant strain of *E. coli*

In our model, the key parameters λ^*_0 and ${\rm IC}^*_{50}$ (defined in Eqs 8 and 9) depend on the translational capacity $\kappa_{\rm t}$. To test the predictions of the model, we used a strain of *E. coli* MG1655 in which the ribosome is mutated such that the peptide elongation rate is decreased [32], with a corresponding decrease in the translational capacity [20]. Measuring the RNA-to-protein ratio, which is proportional to the ribosome concentration ([20]; see Supplementary Material) as a function of growth rate in the absence of antibiotics and using Eq. 4, we found that the translational capacity $\kappa_{\rm t}$ for the mutant is decreased by a factor of 0.65 relative to that of the wildtype, $\kappa_{\rm t}^{\rm MUT} = 0.65\kappa_{\rm t}^{\rm WT}$ (Fig. 6A and Table S5).

For the reversible antibiotic tetracycline, we expect that the ${\rm IC}_{50}$ is well-approximated by the limiting form, ${\rm IC}_{50} = (\kappa_t/\lambda_0) \times K_D \times (P_{\rm out}/P_{\rm in}) \times \Delta r$; thus the ratio of susceptibilities between the wildtype and mutant strains ${\rm IC}_{50}^{\rm WT}/{\rm IC}_{50}^{\rm MUT}$ should be proportional to the ratio of drug-free growth rates $\lambda_0^{\rm MUT}/\lambda_0^{\rm WT}$, with proportionality constant $\kappa_{\rm t}^{\rm WT}/\kappa_{\rm t}^{\rm MUT} = 1/0.65$.

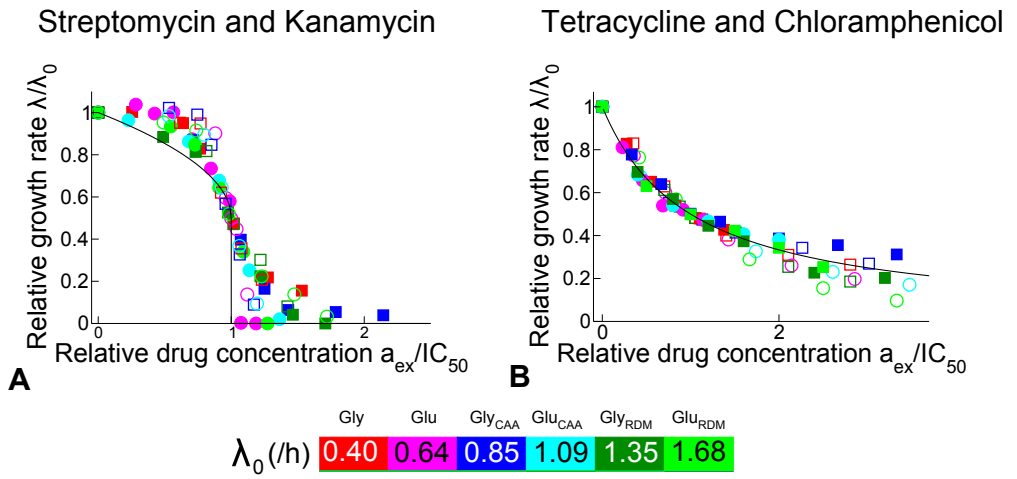

FIG. 5: Growth inhibition curves for our reversibly- and irreversibly-binding drugs collapse onto two qualitatively different limiting forms as predicted by the model. **A**: Data for the irreversible antibiotics streptomycin (closed symbols) and kanamycin (open symbols) collapse onto $\lambda/\lambda_0 = (1/2)[1 + \sqrt{1 - a_{\rm ex}/{\rm IC}_{50}}]$ (black line). **B**: Data for the reversible antibiotics tetracycline (closed symbols) and chloramphenicol (open symbols) collapse onto $\lambda/\lambda_0 = 1/[1 + a_{\rm ex}/{\rm IC}_{50}]$ (black line).

Indeed, when rescaled relative to the IC_{50} of the mutant in minimal media, our results for the wild-type IC_{50} values, measured for our 6 nutrient conditions, do fall on the predicted straight line with gradient 1/0.65 irrespective of carbon source (Fig. 6B; for raw data see Table S6).

We also investigated the response of the translational mutant to the irreversibly-binding drug kanamycin. Here, the situation is more complex because the mutant confers partial resistance to kanamycin (and full resistance to streptomycin), meaning that other molecular parameters are likely to be altered along with $\kappa_{\rm t}$. Nevertheless, growth inhibition curves for the mutant in the presence of kanamycin are well-fitted by our model (Fig. S4).

Mechanistic link between reversibility timescale and growth-dependent susceptibility

Why does our model behave qualitatively differently in the limits where antibiotic transport and binding are irreversible (small λ_0^*) and where they are reversible (large λ_0^*)? In the model,

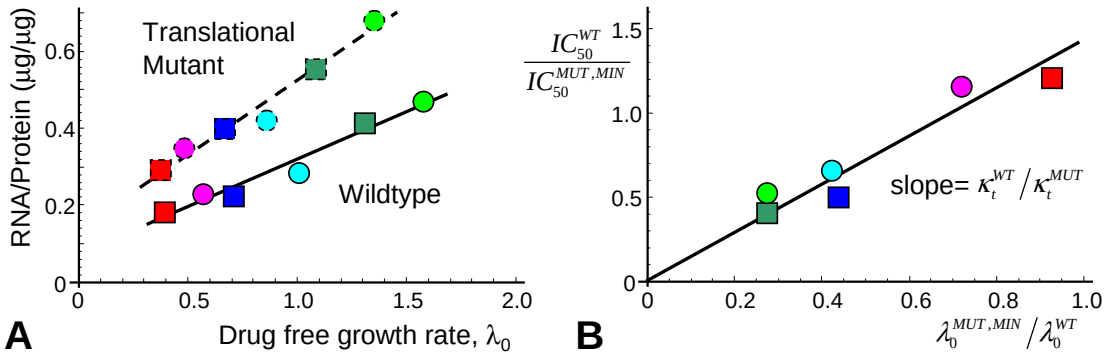

FIG. 6: The translation mutant shows growth-dependent susceptibility to tetracycline in quantitative agreement with the model predictions. **A**: The mutant shows a reduced translational capacity compared to the wildtype strain. Translational capacity is given as the inverse slope of a plot of the RNA/protein ratio versus drug-free growth rate λ_0 (in h^{-1}) [20]. The data for the mutant are from this study (dashed line); wildtype data are taken from Scott *et al.* [20] (solid line). The ratio of slopes (WT/MUT) gives the ratio of translational capacity $\kappa_t^{\rm MUT}/\kappa_t^{\rm WT} = 0.65$ (Table S5). The colored symbols indicate different growth media, as in Fig. 1. **B**: Growth-dependent susceptibility to tetracycline for the translation mutant. The model predicts that for a reversible drug such as tetracycline, $\rm IC_{50} = IC_{50}^{*}\lambda_0^{*}/(2\lambda_0)$, so that $\rm IC_{50}^{WT}/IC_{50}^{MUT} = (\kappa_t^{WT}/\kappa_t^{MUT}) \times (\lambda_0^{MUT}/\lambda_0^{WT}) = (1/0.65) \times (\lambda_0^{MUT}/\lambda_0^{WT})$ (since both λ_0^{*} and $\rm IC_{50}^{*}$ are proportional to $\sqrt{\kappa_t}$). The symbols show $\rm IC_{50}^{WT}$ measured on all 6 growth media, divided by the $\rm IC_{50}^{MUT,MIN}$ measured on glucose minimal or glycerol minimal medium as appropriate, and the drug-free growth rate of the wildtype $\lambda_0^{\rm WT}$ similarly rescaled with respect to the drug-free growth rate of the mutant in the corresponding minimal medium $\lambda_0^{\rm MUT,MIN}$. The data collapse onto a straight line with gradient (1/0.65), as indicated by the solid black line. It is important to note that the solid line is not a line-of-best-fit, but rather comes from taking the ratio of the slopes in panel **A**.

nutrient quality has two opposing influences on the cell's ribosome content: it increases the size of the ribosome pool (solid line in Fig. 2B) but it also reduces the cell's capacity to increase this pool in response to antibiotic challenge (gradient of the dashed lines in Fig. 2B). In other words, fast-growing cells have a ribosome pool which is already close to maximal and have little capacity to increase in response to antibiotic, while slow-growing cells have

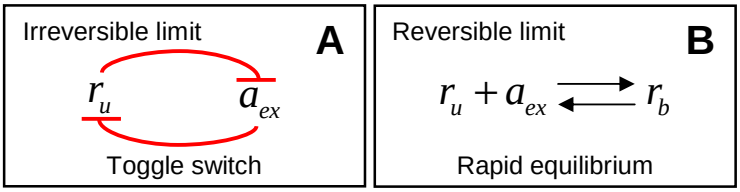

FIG. 7: Shift in the network topology in the irreversible and reversible limits. **A.** In the limit that either transport or binding are irreversible (as is the case for streptomycin and kanamycin), the system exhibits a 'toggle-switch' topology, leading to a steep inhibition curve (Eq. 11). **B.** In the limit of fully-equilibrated transport and binding (as is the case for tetracycline and chloramphenicol), the model predicts more gradual inhibition (Eq. 12).

a small ribosome pool that can be increased by a large factor in response to antibiotic.

In the limit that either transport or binding are irreversible (small λ_0^*), antibiotic molecules that enter the cell are neutralized by binding to free ribosomes, such that the intracellular antibiotic concentration remains low. The model exhibits a 'toggle-switch' topology (Fig. 7A), in which free ribosomes "soak up" antibiotic, while antibiotic inactivates free ribosomes. If the extracellular antibiotic concentration $a_{\rm ex}$ is below a threshold determined by the initial (unbound) ribosome concentration, the cell generates ribosomes fast enough to neutralize all the antibiotic that enters the cell. If, however, $a_{\rm ex}$ exceeds the threshold, the cell's rate of ribosome generation cannot compete with the antibiotic influx and the system flips to a different steady-state with no free ribosomes and correspondingly no growth. Thus in the irreversible limit the fate of a cell is determined by a "molecular race" between antibiotic influx and ribosome production, in which the absolute number of ribosomes is decisive. Fast-growing cells (on rich nutrient) have a larger ribosome pool and correspondingly higher ribosome synthesis rate, so that they are able to tolerate a higher rate of antibiotic influx than slow-growing cells.

In contrast, in the limit of fully-reversible transport and binding (large λ_0^*), the free and bound ribosome pools are in equilibrium (Fig. 7B), and the intra- and extra-cellular antibiotic pools are also in equilibrium. Increasing the antibiotic concentration shifts the equilibrium between free and bound ribosome pools; the cell responds by increasing the total ribosome pool (dashed line in Fig. 2B). This leads to a smoothly-varying,

Langmuir-like dependence of the relative growth rate λ/λ_0 on the extracellular antibiotic concentration $a_{\rm ex}$. Because λ/λ_0 is determined by the *relative* sizes of the ribosome pool in the presence and absence of antibiotic, the half-inhibition concentration depends on the slope of the dashed line in Fig. 2B. Slow-growing cells have more capacity to increase their ribosome pool (steeper slope of the dashed line; Fig. 2B), and as a consequence they are less susceptible to antibiotic than fast-growing cells.

Discussion

Taken together, our results show that bacterial susceptibility to ribosome-targeting antibiotics exhibits strong growth-rate dependence, but that the nature of this dependence differs qualitatively between antibiotics (Fig. 1). For irreversibly-binding antibiotics (streptomycin and kanamycin), slower growing cells are more susceptible; whereas for reversibly-binding antibiotics (tetracycline and chloramphenicol), faster growing cells are more susceptible. This behaviour can be understood by a simple mechanistic model which shows that these contrasting effects of nutrient environment on susceptibility for different antibiotics can be explained in terms of a single parameter, the critical reversibility rate λ_0^* (Eq. 8), which characterizes the outward permeability and binding affinity of the drug.

Our model predicts a parameter-free relation for the growth-dependent susceptibility (Eq. 10), *i.e.* how the IC_{50} depends upon the drug-free growth rate λ_0 relative to the critical reversibility rate λ_0^*. This relation is in very good agreement with the experimental data (Fig. 4). If the pathogen drug-free growth rate λ_0 is larger than λ_0^* the IC_{50} increases with drug-free growth rate (as it does for our irreversible antibiotics streptomycin and kanamycin), so that slow-growing cells are more susceptible. In contrast, if the pathogen drug-free growth rate is smaller than λ_0^* (as for our reversible antibiotics tetracycline and chloramphenicol) the IC_{50} decreases with drug-free growth rate, so that fast-growing cells are more susceptible. Our model also predicts very different shapes for the growth-inhibition curves in these two cases; if $\lambda_0 > \lambda_0^*$ (as for our irreversible drugs), the growth-inhibition curves show a sharp drop around the IC_{50}, while if $\lambda_0 < \lambda_0^*$ (as for our reversible drugs), we expect smoothly varying growth-inhibition curves. Moreover, in the reversible and irreversible limits of large and small λ_0^*, our model leads to parameter-free predictions for both growth-dependent susceptibility (Eq. 10) and growth inhibition curves (Eqs. 11 and

12), which are confirmed by a collapse of the data points on the predicted re-scaled curves (Fig. 5). Finally, the insight provided by our analysis allows us to make sucessful predictions for how antibiotic susceptibility is modified by a mutation affecting translation rate (Fig. 6).

Significance of the critical reversibility rate λ_0^*

A major insight arising from this study is the importance of the critical reversibility rate λ_0^* in determining susceptibility to antibiotic treatment. For a given ribosome-targeting antibiotic and pathogenic strain, λ_0^* can be inferred from known biochemical parameters (via Eq. 8) in cases where these are known, or, alternatively, estimated by measuring inhibition curves over a range of drug-free growth rates (a task well-suited to automation [33]). This critical reversibility rate provides a spectrum classification of ribosome-targeting antibiotics according to their physiological effects, which, interestingly, appears to correlate at its extremes with existing binary classification schemes, at least for the antibiotics used in this study. In particular, the irreversible antibiotics streptomycin and kanamycin are classified as bactericidal, whereas the reversible antibiotics tetracycline and chloramphenicol are classified as bacteriostatic. This is consistent with the fact that our model predicts a rapidly-vanishing growth rate beyond the IC_{50} for irreversible antibiotics (*i.e.* those with small values of λ_0^*). Our classification on the basis of λ_0^* also correlates with the fact that streptomycin and kanamycin are known to transiently induce expression of proteins associated with heat-shock in *E. coli*, whereas tetracycline and chloramphenicol induce expression of proteins associated with cold-shock [34]. It remains to be seen whether these responses are triggered directly by the antibiotic or are associated more generally with physiological changes occurring in the organism.

Coupling of cell physiology and antibiotic mode-of-action

In a wider context, bacterial growth rate is an important factor controlling gene expression and regulation [21, 23], imposing strong constraints on the allocation of cellular resources. These constraints lead to intrinsic growth-rate dependence in the macromolecular composition of the cell [20, 35]. Consequently, it is to be expected (and in some cases it is known [9–11, 36]) that antibiotic susceptibility likewise exhibits growth-rate dependence for those drugs targeting key cellular resources such as the ribosome, RNA polymerase, DNA gyrase,

and cell wall biosynthetic machinery. Our results show that for ribosome-targeting antibiotics, complex growth-rate dependent susceptibility can arise from the interplay between molecular mechanism (antibiotic transport and binding) and cellular physiology (growth-dependent constraints on ribosome concentration and synthesis rate). Interestingly, our work shows that knowledge of the growth-rate dependence of the target (here, the ribosome) is not sufficient to predict the growth-rate dependence of the antibiotic susceptibility – in fact, the nature of this dependence differs qualitatively among antibiotics despite their common target (Fig. 1). Nonetheless, contrasting patterns of growth rate-dependent susceptibility can be explained quantitatively by combining mechanistic details of antibiotic mode-of-action with empirically determined physiological constraints.

At higher concentrations than those considered here ($\sim 10\times$ IC_{50}), other mechanisms have been implicated in the inhibition of bacterial growth by ribosome-targeting antibiotics. These include changes in the transmembrane proton-motive force, membrane permeabilization by misfolded protein [14], induction of a heat-shock response [37], and, on longer time scales, oxidative stress which increases mutation rate and accelerates the emergence of resistance [38]. A complete picture of antibiotic action will require integration of specific response mechanisms, such as these, with general constraints imposed by pathogen growth, although the simple model presented here appears to capture the majority of the growth-dependent susceptibility to the ribosome-targeting antibiotics tested. Applying a similar approach to other classes of antibiotics or chemotherapeutic agents should provide a clearer picture of *in vivo* drug action.

Clinical and evolutionary perspectives

From a clinical perspective, the strong positive correlation of the IC_{50} with drug-free growth rate that we observe for our irreversibly-binding antibiotics suggests that the efficacy of treatment could be improved by modulating the bacterial growth rate using a metabolic inhibitor – echoing recent developments in understanding the role of nutrient environment in overcoming persistent infections [8]. The threshold-like transition in the inhibition curve for irreversibly-binding antibiotics can, however, greatly facilitate acquisition of resistance, especially in the presence of steep spatial gradients of antibiotic [3, 5, 39], providing yet another caution against their improvident use [40]. More broadly, it is becoming clear

that understanding and manipulating pathogen physiology plays a major role in improving strategies for the eradication of infection. Although both drug action and pathogen metabolism are mechanistically complex, the interplay between molecular interactions and whole-cell physiology can nevertheless be understood quantitatively using simple rules.

Methods

Antibiotics

Antibiotics were obtained from Fisher Scientific: Streptomycin sulfate (BP910-50), Kanamycin Sulfate (BP906-5), Tetracycline hydrochloride (BP912-100) and Chloramphenicol (BP904-100). Stock solutions were prepared weekly, and stored at 4 °C. To avoid degradation of the antibiotics (particularly tetracycline), cultures were grown no longer than 6 hours before transfer to medium containing fresh antibiotic and all experiments were performed in light-insulated shakers.

Growth media

The growth media is potassium morpholinopropane sulfonate (MOPS) buffered, and is a modification of Neidhardt supplemented MOPS defined media [25] obtained from Teknova (M2101). Carbon sources used were glycerol (0.2% v/v) and glucose (0.2% w/v). Intermediate growth rates were obtained by supplementing glycerol and glucose minimal media with casamino acids (0.2% w/v). The most rapid growth rates were obtained by supplementing the media with nucleotides (Teknova, M2103) and all amino acids (Teknova, M2104).

Strains and growth conditions

Escherichia coli K12 strain MG1655 was used in this study. Seed cultures were grown in LB medium (Bio Basic), and used to inoculate pre-cultures in appropriate growth media without antibiotics. After over-night growth, pre-cultures were diluted ($500 - 1000\times$) to fresh media and allowed to resume exponential growth for at least three generations before being diluted into media containing antibiotics. Cells were adapted to exponential growth in antibiotics and grown in adapted growth for four generations before growth rate measurements were taken. Cells were grown in 3 mL of culture media at 37 °C in 20 mm test

tubes, shaken in a water bath (MaxQ 7000, Thermo-Fisher) at 250 rpm. Growth rate was monitored by measuring OD_{600} on a Biomate 3S spectrophotometer (Thermo-Fisher) over time, with cell viability corroborated by plating. The translational mutant strain appearing in Fig. 6 is a *rpsL* point mutation that confers pseudo-dependence on streptomycin [20, 32], moved from strain GQ9 [20] (also known as CH349 or UK317 [32]) into our wild type background via P1 transduction.

Protein and RNA extraction

Total protein was determined using a modified Lowry method (Sigma, TP0300) [41, 42], with bovine serum albumin as a standard. RNA quantification was done via cold perchloric acid precipitation [43].

Data fits

Estimates for the critical parameter combinations λ_0^* and IC_{50}^* were obtained by fitting the experimental growth inhibition curves $\lambda(a_{\mathrm{ex}})$ to the solution of the cubic equation, Eq. 7. These fits were carried out using Powell's method [44].

Acknowledgments

We thank L. Ciandrini and M. C. Romano for discussions and B. Waclaw, M. E. Cates, P. B. Warren, P. Swain, S. Klumpp, T. Bollenbach and R. Beardmore for comments on the manuscript. This work was partially supported by EPSRC under grant EP/J007404/1. PG was funded by a DAAD postdoc fellowship and a DFG research fellowship. RJA was supported by a Royal Society University Research Fellowship. MS was supported by a Discovery grant through the Natural Sciences and Engineering Research Council of Canada.

Author contributions

P.G. and M.S. contributed equally to this work. M.S. performed the experiments. All authors contributed extensively to the experimental and model design, analysis of data and writing of the paper.

Additional information

The authors declare no competing financial interests.

Figure legends

Figure 1

Antibiotic susceptibility depends on nutrient quality for four ribosome-targeting antibiotics: irreversibly-binding antibiotics streptomycin (**A** & **B**) and kanamycin (**C** & **D**), and reversibly-binding antibiotics tetracycline (**E** & **F**) and chloramphenicol (**G** & **H**). The left panels show the growth rate λ of *E. coli* MG1655 relative to the drug-free growth rate λ_0, as a function of the antibiotic concentration. Growth inhibition data are shown for media with glycerol as the carbon source. The arrows indicate increasing drug-free growth rate λ_0. The right panels show the half-inhibition concentration IC_{50} as a function of the drug-free growth rate λ_0. Carbon sources are denoted by symbol: glucose (circles), glycerol (squares), and error bars denote the standard deviation among repeated measurements (Tables S2 and S3). Media are variants of Neidhardt's MOPS buffered medium [25]; see Methods for details.

Figure 2

Schematic view of the model and its dynamics. **A.** The model is focused on three state variables: the intracellular concentration of antibiotic a, the concentration r_u of ribosomes unbound by antibiotic and the concentration r_b of antibiotic-bound ribosomes. Two mechanisms drive the dynamics: 1. *Transport* across the cell membrane and 2. *Binding* of ribosomes and antibiotic. **B.** Constraints arising from empirical relations between ribosome content and growth rate. Scott *et al.* [20] measured total ribosome content as a function of growth rate. When growth rate is varied by nutrient composition, in the absence of antibiotics, ribosome content r_u correlates positively with growth rate λ, increasing linearly from a minimum concentration of inactive ribosomes r_min (solid line). When growth rate is decreased by imposing translational inhibition, total ribosome content $r_\mathrm{tot} = r_\mathrm{u} + r_\mathrm{b}$ increases, reaching a maximum r_max as growth rate decreases to zero (dashed lines). Note that Scott *et al.* measured ribosome mass fraction; here we translate these to concentrations (see Supplementary Information, Fig. S1).

Figure 3

Model fits to growth inhibition curve data. The parameters λ_0^* and IC_{50}^* are obtained by numerical fitting of the solution of the cubic equation, Eq. 7, to our experimental growth inhibition curves. Data sets for different drug-free growth rates (*i.e.* the different curves in each panel) were fitted simultaneously with the same values of λ_0^* and IC_{50}^*, but separate fits were obtained for glycerol-based and glucose-based media. Here we show the resulting fits for glycerol-based media (symbols as in Fig. 1. of the main text). The parameters obtained by this procedure are: Streptomycin, glycerol: $\lambda_0^* = 0.31\mathrm{h}^{-1}$, $\mathrm{IC}_{50}^* = 0.19\mu$g/ml, streptomycin, glucose: $\lambda_0^* = 0.57\mathrm{h}^{-1}$, $\mathrm{IC}_{50}^* = 0.36\mu$g/ml, kanamycin, glycerol: $\lambda_0^* = 0.17\mathrm{h}^{-1}$, $\mathrm{IC}_{50}^* = 0.05\mu$g/ml, kanamycin, glucose: $\lambda_0^* = 0.47\mathrm{h}^{-1}$, $\mathrm{IC}_{50}^* = 0.26\mu$g/ml, tetracycline, glycerol: $\lambda_0^* = 5.2\mathrm{h}^{-1}$, $\mathrm{IC}_{50}^* = 0.23\mu$M, tetracycline, glucose: $\lambda_0^* = 6.3\mathrm{h}^{-1}$, $\mathrm{IC}_{50}^* = 0.36\mu$M, chloramphenicol, glycerol: $\lambda_0^* = 1.8\mathrm{h}^{-1}$, $\mathrm{IC}_{50}^* = 2.5\mu$M, chloramphenicol, glucose: $\lambda_0^* = 1.5\mathrm{h}^{-1}$, $\mathrm{IC}_{50}^* = 4.1\mu$M. These values of λ_0^* and IC_{50}^* are compared to literature data in Table S4. Similar results are obtained if we instead fit our data directly to the predicted universal relation for $\mathrm{IC}_{50}(\lambda_0)$ (Eq. 10); see Supplementary Information and Fig. S3.

Figure 4

Universal growth-dependent susceptibility curve. Data from the right panels of Fig. 1 are rescaled by λ_0^* and IC_{50}^*, obtained by fitting our growth inhibition data (Fig. 3). The black line shows the model prediction for the universal curve, Eq. 10.

Figure 5

Growth inhibition curves for our bactericidal and bacteriostatic drugs collapse onto two qualitatively different limiting forms as predicted by the model. **A**: Data for the bactericidal antibiotics streptomycin (closed symbols) and kanamycin (open symbols) collapse onto $\lambda/\lambda_0 = (1/2)[1 + \sqrt{1 - a_{\mathrm{ex}}/\mathrm{IC}_{50}}]$ (black line). **B**: Data for the bacteriostatic antibiotics tetracycline (closed symbols) and chloramphenicol (open symbols) collapse onto $\lambda/\lambda_0 = 1/[1 + a_{\mathrm{ex}}/\mathrm{IC}_{50}]$ (black line).

Figure 6

The translation mutant shows growth-dependent susceptibility to tetracycline in quantitative agreement with the model predictions. **A**: The mutant shows a reduced translational

capacity compared to the wildtype strain. Translational capacity is given as the inverse slope of a plot of the RNA/protein ratio versus drug-free growth rate λ_0 [20]. The data for the mutant are from this study (dashed line); wildtype data are taken from Scott *et al.* [20] (solid line). The ratio of slopes (WT/MUT) gives the ratio of translational capacity $\kappa_t^{\rm MUT}/\kappa_t^{\rm WT} = 0.65$ (Table S5). The colored symbols indicate different growth media, as in Fig. 1. **B**: Growth-dependent susceptibility to tetracycline for the translation mutant. The model predicts that for a reversible drug such as tetracycline, IC_{50} =$\mathrm{IC}_{50}^{*}\lambda_0^{*}/(2\lambda_0)$, so that $\mathrm{IC}_{50}^{\rm WT}/\mathrm{IC}_{50}^{\rm MUT} = (\kappa_t^{\rm WT}/\kappa_t^{\rm MUT}) \times (\lambda_0^{\rm MUT}/\lambda_0^{\rm WT}) = (1/0.65) \times (\lambda_0^{\rm MUT}/\lambda_0^{\rm WT})$ (since both λ_0^{*} and IC_{50}^{*} are proportional to $\sqrt{\kappa_t}$). The symbols show $\mathrm{IC}_{50}^{\rm WT}$ measured on all 6 growth media, divided by the $\mathrm{IC}_{50}^{\rm MUT,MIN}$ measured on glucose minimal or glycerol minimal medium as appropriate, and the drug-free growth rate of the wildtype $\lambda_0^{\rm WT}$ similarly rescaled with respect to the drug-free growth rate of the mutant in the corresponding minimal medium $\lambda_0^{\rm MUT,MIN}$. The data collapse onto a straight line with gradient (1/0.65), as indicated by the solid black line. It is important to note that the solid line is not a line-of-best-fit, but rather comes from taking the ratio of the slopes in panel **A**.

Figure 7

Shift in the network topology in the irreversible and reversible limits. **A.** In the limit that either transport or binding are irreversible (as is the case for streptomycin and kanamycin), the system exhibits a 'toggle-switch' topology, leading to a steep inhibition curve (Eq. 11). **B.** In the limit of fully-equilibrated transport and binding (as is the case for tetracycline and chloramphenicol), the model predicts more gradual inhibition (Eq. 12).

[1] A. Y. Peleg and D. C. Hooper, New Eng. J. Med. **362**, 1804 (2010).

[2] P. Greulich, B. Waclaw, and R. J. Allen, Phys. Rev. Lett. **109**, 088101 (2012).

[3] R. Hermsen, J. B. Deris, and T. Hwa, Proc. Natl. Acad. Sci. USA **109**, 10775 (2012).

[4] A. Rodríguez-Rojas, J. Rodríguez-Beltrán, A. Couce, and J. Blázquez, Int. J. Med. Microbiol. **303**, 293 (2013).

[5] J. B. Deris, M. Kim, Z. Zhang, H. Okano, R. Hermsen, A. Groisman, and T. Hwa, Science **342**, 1237435 (2013).

[6] D. Davies, Nat. Rev. Drug Discov. **2**, 114 (2003).

[7] K. Lewis, Nat. Rev. Microbiol. **5**, 48 (2007).

[8] K. R. Allison, M. P. Brynildsen, and J. J. Collins, Nature **473**, 216 (2011).

[9] R. M. Cozens, E. Tuomanen, W. Tosch, O. Zak, J. Suter, and A. Tomasz, Antimicrob. Agents Ch. **29**, 797 (1986).

[10] E. Tuomanen, R. Cozens, W. Tosch, O. Zak, and A. Tomasz, J. Gen. Microbiol. **132**, 1297 (1986).

[11] M. R. Millar and J. Pike, Antimicrob. Agents Ch. **36**, 185 (1992).

[12] A. Yonath, Annu. Rev. Biochem. **74**, 649 (2005).

[13] J. Poehlsgaard and S. Douthwaite, Nat. Rev. Microbiol. **3**, 870 (2005).

[14] B. D. Davis, Microbiol. Rev. **51**, 341 (1987).

[15] T. R. Tritton, Biochemistry **16**, 4133 (1977).

[16] D. Nierhaus and K. H. Nierhaus, Proc. Natl. Acad. Sci. U S A **70**, 2224 (1973).

[17] R. J. Harvey and A. L. Koch, Antimicrob. Agents Ch. **18**, 323 (1980).

[18] H. Bremer and P. Dennis, in *E. coli and S. Typhimurium: Cellular and Molecular Biology*, edited by F. C. Neidhardt (ASM Press, 1996).

[19] O. Maaloe, in *Biological Regulation and Development*, edited by R. F. Goldberger (Plenum, New York, 1979).

[20] M. Scott, C. W. Gunderson, E. M. Mateescu, Z. Zhang, and T. Hwa, Science **330**, 1099 (2010).

[21] C. You, H. Okano, S. Hui, Z. Zhang, M. Kim, C. W. Gunderson, Y.-P. Wang, P. Lenz, D. Yan, and T. Hwa, Nature **500**, 301 (2013).

[22] M. Scott and T. Hwa, Curr. Op. Biotech. **22**, 559 (2011).

[23] S. Klumpp, Z. Zhang, and T. Hwa, Cell **139**, 1366 (2009).

[24] S. Klumpp and T. Hwa, Curr. Op. Biotech. **28**, 96 (2014).

[25] F. Neidhardt, P. L. Bloch, and D. F. Smith, J. Bacteriol. **119**, 736 (1974).

[26] S. Klumpp, M. Scott, S. Pedersen, and T. Hwa, Proc. Natl. Acad. Sci. USA **110**, 16754 (2013).

[27] C. Berens, in *RNA-Binding Antibiotics*, edited by R. Schroeder (Landes Bioscience, 2001).

[28] T. J. Franklin and G. A. Snow, in *Biochemistry and Molecular Biology of Antimicrobial Drug Action* (Springer, 2006).

[29] M. Misumi, T. Nishimura, T. Komai, and N. Tanaka, Biochem. Biophys. Res. Commun. **84**, 358 (1978).

[30] J. Elf, K. Nilsson, T. Tenson, and M. Ehrenberg, Phys. Rev. Lett. **97**, 1 (2006).

[31] D. Fange, K. Nilsson, T. Tenson, and M. Ehrenberg, Proc. Natl. Acad. Sci. USA **106**, 1 (2009).

[32] T. Ruusala, D. Andersson, M. Ehrenberg, and C. G. Kurland, EMBO J. **3**, 2575 (1984).

[33] T. Bollenbach and R. Kishony, Mol. Cell **42**, 413 (2011).

[34] R. A. Van Bogelen and F. C. Neidhardt, Proc. Natl. Acad. Sci. **87**, 5589 (1990).

[35] R. E. Ecker and M. Schaechter, Annals of the New York Academy of Sciences **102**, 549 (1962).

[36] A. L. Koch and G. H. Gross, Antimicrob. Agents Ch. **15**, 220 (1979).

[37] C. Tan, R. P. Smith, J. K. Srimani, K. A. Riccione, S. Prasada, M. Kuehn, and L. You, Mol. Syst. Biol. **8**, 617 (2012).

[38] M. A. Kohanski, M. A. DePristo, and J. J. Collins, Mol. Cell **37**, 311 (2010).

[39] Q. Zhang, G. Lambert, D. Liao, H. Kim, K. Robin, C.-K. Tung, N. Pourmand, and R. H. Austin, Science **333**, 1764 (2011).

[40] G. A. Pankey and L. D. Sabath, Clinical Infectious Diseases **38**, 864 (2004).

[41] O. H. Lowry, N. J. Rosebrough, A. L. Farr, and R. J. Randall, J. Biol. Chem. **193**, 265 (1951).

[42] G. L. Peterson, Anal. Biochem. **100**, 201 (1979).

[43] S. Benthin, J. Nielsen, and J. Villadsen, Biotechnol. Techniques **5**, 39 (1991).

[44] W. H. Press, S. A. Teukolsky, W. T. Vetterling, and B. P. Flannery, *Numerical Recipes in C* (Cambridge University Press, 1992), 2nd ed.